J. Min. Metall. Sect. B-Metall. 51 (1) B (2015) 73 - 79

Journal of Mining and Metallurgy, Section B: Metallurgy

STUDY ON STRENGTH AND FRACTURE TOUGHNESS OF Al–Zn–Mg–Cu–Ti(–Sn) ALLOYS

A. Yan [a], L. Chen [a], H.S. Liu [a,*], F.F. Xiao [a], X.Q. Li [b]

[a] School of Materials Science and Engineering, Central South University, Changsha, China
[b] School of Mechanical and Electric Engineering, Central South University, Changsha, China

(Received 22 January 2013; accepted 21 November 2014)

Abstract

The strength and fracture toughness of Al–Zn–Mg–Cu–Ti(–Sn) alloys were investigated by performing tensile and plane strain fracture toughness (K_{IC}) tests. Detailed observations with optical, scanning electron and transmission electron microscopy were conducted to analyze microstructure and fracture surfaces of the alloys. The results revealed that addition of Sn refined the solution-aging grain size of matrix and reduced coarsening rate of precipitate during aging. Narrower precipitation free zones and more discontinuous distribution of grain boundary precipitates were observed to be displayed in the Sn-containing alloy. Small size second phase particles Mg_2Sn were observed to form in the Sn-containing alloy and distribute in the fine dimples of fracture surface. These features of microstructure were believed to impart higher strength and fracture toughness of the Sn-containing alloy on overaging.

Keywords: Strength, Fracture toughness, Sn, Microstructure, Al–Zn–Mg–Cu

1. Introduction

As an important high strength aluminium alloy, 7000 series (Al–Zn–Mg–Cu) alloy has become one of the most potential structural materials in the aerospace field [1-3]. However, in aerospace design, fracture toughness is a critical parameter when taking damage tolerant concept into consideration. As high-strength is known to be detrimental to toughness, it undoubtedly hampers the extensive development and utilization of high-strength 7000 series aluminium alloys [4]. Therefore, a good compromise between strength and fracture toughness is required. To satisfy this requirement, multiple investigations have been carried out on fracture toughness of the 7000 series aluminium alloy, which are relevant to analyze influences of strength and microstructural conditions related to strength on toughness [5-8]. The microstructural features are known to exert significant effects on strength and fracture toughness. Microstructural control as a viable way to enhance these two properties focused of much research effort.

Generally, microalloying is a primary and key method to control the structure of grain, grain boundary *etc*. For example, addition of Sc to Al–Zn–Mg–Cu alloys can produce an Al_3Sc dispersoid, which is beneficial to mechanical and fatigue properties [9-11]. Synergistic advantages are known to accrue when Sc is added together with Zr, owing to the formation of secondary fine coherent Al_3(Sc,Zr) dispersoids [12]. Although Sc is a known grain refiner in Al alloys, its scarcity and security of supply have so far precluded its widespread use. Instead, much attention has been focused on the addition of the rare earth element (RE). Peng *et al*. [13] investigated the effect of Cr and Yb additions on strength and fracture toughness of Al–Zn–Mg–Cu–Zr alloy, and pointed out that both strength and fracture toughness of Al–Zn–Mg–Cu–Zr alloy could be enhanced owing to the improvement of recrystallization resistance caused by the additions of Cr and Yb. In recent years, Li-containing aluminium alloys have been intensively investigated for their advantages of high-specific strength and modulus and low density. Bai *et al*. [14] and Huang *et al*. [15] studied the effects of Li addition on aging responses of Al–Zn–Mg–Cu alloy, and reported that Li promotes the precipitation of homogenously distributed fine η′ ($MgZn_2$) phases and narrows the precipitation-free zones. Whereas, when the content of Li is high (>1.7 wt-%), δ′ (Al_3Li) phase, instead of η′, will be dominant, which may result in weak properties for the well-known reason that η′ phases lead to the most significant improvement of mechanical properties in 7000 series alloys.

Addition of Sc, RE and Li element to Al alloys is not economically feasible in practice. As an alternative, some attention has been focused on the element Sn, which is much less expensive. The beneficial effects of the addition of Sn to Al–Cu based

* *Corresponding author: hsliu@csu.edu.cn*

DOI:10.2298/JMMB130122003Y

alloys and Al–Si–Mg alloy have been the subject of many studies [16-19]. It is reported that indicated that trace addition of Sn to Al–Cu–Mg alloy resulted in finer and more dispersed θ′ precipitates and also reduced the misfit of the precipitate with the Al matrix, results in improved tensile strength and toughness of the studied alloy [18].

The present authors found that addition of Sn reinforces the propagation resistance of fatigue crack of overaged Al–Zn–Mg–Cu alloy [20]. In this paper, the effect of Sn addition on aging hardening behavior and fracture toughness of the Al–Zn–Mg–Cu–Ti alloy were studied to reveal the role of Sn in strength and fracture toughness.

2. Experimental

2.1 Sample preparation and heat treatment

The actual compositions of the Al–Zn–Mg–Cu alloys used in the present study are listed in Table 1. The compositions of the investigated alloys are similar to that of AA 7050 alloy. The starting materials included pure Al (99.99 wt.%), Mg (99.9 wt.%), Zn (99.9 wt.%) and Sn (99.9 wt.%) bulks, and Al-52 wt.% Cu and Al-2.7 wt.% Ti master alloys. The alloys used in this study were prepared as follows. First, the weighted starting materials were melted and refined in an electric resistance furnace at 750~780°C and were then casted into a rectangular ingot with dimensions of 270 × 135 × 32 mm.

Table 1. *Actual compositions of studied Al–Zn–Mg–Cu–Ti (–Sn) alloys (wt.%).*

Alloys	Zn	Mg	Cu	Ti	Sn	Al
Sn-free	6.08	2.08	2.1	0.1	–	Bal.
Sn-containing	6.13	2.11	2.06	0.1	0.1	Bal.

The ingots of Al–Zn–Mg–Cu–Ti(–Sn) alloys were subjected to homogenization and subsequent air cooling to room temperature, and they were then scalped and hot-rolled at about 420°C. Two kinds of rolling plates were prepared here: (1) the ingots hot-rolled to 11.0 mm to form thick plates; (2) the ingots hot-rolled to 3.0 mm firstly, and subsequent cold-rolled to form thin plates with a thickness of 2.0 mm. These two kinds of plates were solution-treated in a salt bath at 470°C for 1 h and water-quenched to room temperature. Single-stage aging treatment was performed for 2.0 mm thin plates at 120 °C for 4, 8, 12, 16, 20, 24, 28, 32, 36, 42, 48, 54 and 60 h, respectively. Meanwhile, the thick plates were double-aged at 120°C × 24 h + 175°C × 10 h, similar to the condition of T76, one of the most common service states for 7000 series aluminium alloy.

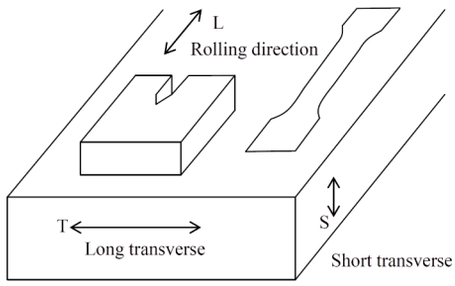

Figure 1. *Specimen orientations used for tensile tests and fracture toughness tests.*

2.2 Tensile and fracture toughness tests

The tensile testing specimens for age hardening curves were taken in the longitudinal (L) orientation (*i.e.*, parallel to the rolling direction) of the thin plates with gauge length 50 mm and 2.0 mm thick. The ambient temperature tensile properties tests were performed on CSS-44100 electronic universal testing machine at a tensile velocity of 2 mm min^{-1}.

Failure-safe design is based on valid plane-strain fracture toughness (K_{IC}) values. Generally, this property is measured with stress state near the crack front as plane strain and confined plasticity. If these conditions are valid, the K_{IC} value represents a lower limiting value of fracture toughness, which leads to a very conservative design and estimation of failure stress and critical defect size for a material in service under similar stress state conditions [21]. The plane-strain fracture toughness tests were performed on compact tension specimens taken from the thick plates in the T–L orientation with a size (in mm) of 48×40×10 (L×W×B) in accordance with the ASTM standard E-399 [22]. Tests were carried out on an MTS 810 servo hydraulic machine. In order to obtain fracture toughness test parameters, the tensile test of rod specimens taken in the L orientation of the thick plates should be carried out before. Specimen orientations used for tensile tests and fracture toughness tests are shown in Fig. 1.

2.3 Microstructure and differential scanning calorimetry analysis

Microstructure of the samples was observed and examined with optical microscopy, scanning electron microscopy (SEM, Quanta 200) and X-ray diffractometry (XRD, Rigaku D/max 2500). Fracture surface of the compact-tension specimens was also analyzed by SEM. Transmission electron microscopy (TEM) was employed to characterize microstructure of the aged Al–Zn–Mg–Cu–Ti alloys with and without Sn.

The samples for TEM analysis were prepared as

follows. First, they were mechanically ground down to 80 μm, then cut into slices with a diameter of 3 mm, and subsequently electropolished in a solution of 30% nitric acid and 70% methanol maintained at -20°C to -35°C under a voltage of 15 V. Following these steps, the slices were cleaned in ethanol at room temperature for at least 5 min. They were then examined on a JEM 2100F TEM machine operating at 200 kV.

In order to further analyze the precipitation kinetics of the strengthening phases, Differential Scanning Calorimetry (DSC) was carried by using a NERZSCH DSC200F system. For DSC measurement, slices of 0.5mm thickness were cut and punched to obtain 5 mm diameter discs, and then heated in a flowing argon atmosphere from room temperature to 400 °C with a constant heating rate of 10 °C min^{-1}.

3. Results

3.1 Tensile properties

Precipitation responses of the experimental alloys are revealed by aging hardening curves. Tensile strength and elongation of Al–Zn–Mg–Cu–Ti(–Sn) rolled thin plate after single aging at 120 °C for different durations were measured as presented in Fig. 2. It can be seen that the peak strength (pointed by arrows) of the rolled plate of Al–Zn–Mg–Cu–Ti alloy reaches 574 MPa after aging for 24 h with elongation of 13.8%, while the Al–Zn–Mg–Cu–Ti–Sn rolled plate reaches its peak strength of 568 MPa, slight lower than that of the alloy without Sn, after aging for 28 h, but with higher elongation up to 15.1%. Additionally, the overaged softening rate of Sn-containing alloy is slower. For example, after aging for 48 h, the ultimate strength of Al–Zn–Mg–Cu–Ti–Sn alloy remains 563 MPa, while the strength of Al–Zn–Mg–Cu–Ti alloy decreases to 557 MPa. It is demonstrated that the Al–Zn–Mg–Cu–Ti–Sn alloy can get a higher strength on overaged condition.

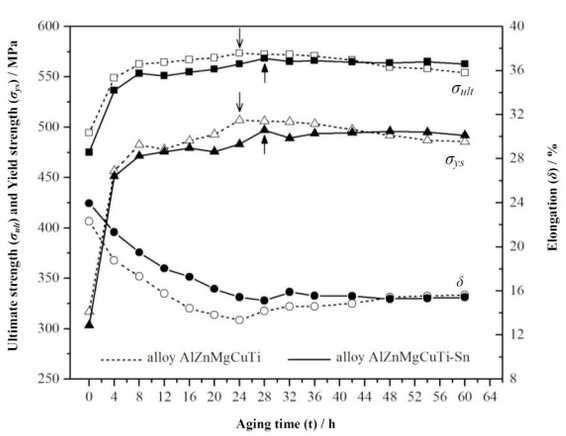

Figure 2. *Mechanical properties changing with aging time at 120 °C for rolled plate*

3.2 Fracture toughness

Fracture toughness (K_{IC}) and tensile properties of the double-aged specimens taken from thick plates are listed in Table 2. As seen, the average fracture toughness values of Sn-containing and Sn-free samples are 33.2 MPa $m^{1/2}$ and 31.4 MPa $m^{1/2}$, respectively. The Sn-containing sample possesses higher fracture toughness. Meanwhile, as listed in Table 2, the double-aged Al–Zn–Mg–Cu–Ti–Sn alloy has higher ultimate strength and yield strength, which is consistent with the results that Sn-containing alloy can get a higher strength on overaged condition as illustrated in Fig.2. Therefore, it is concluded that Sn addition can improve the fracture toughness of Al–Zn–Mg–Cu–Ti alloy by 6% under overaged condition, without sacrificing strength.

Table 2. *Mechanical properties and fracture toughness of double-aged Al–Zn–Mg–Cu–Ti(–Sn) alloys*

Alloys	σ_{ult} / MPa	σ_{ys} / MPa	δ / %	$^{*}K_{IC}$ / MPa $m^{1/2}$
Al–Zn–Mg–Cu–Ti	$482^{\pm 3}$	$420^{\pm 3}$	$15.8^{\pm 0.2}$	$31.4^{\pm 0.2}$
Al–Zn–Mg–Cu–Ti–Sn	$498^{\pm 3}$	$431^{\pm 4}$	$15.3^{\pm 0.2}$	$33.2^{\pm 0.3}$

* *The fracture toughness tests were conducted by three valid samples for each alloy.*

4. Discussion

The present results demonstrate that addition of Sn is beneficial to increase strength and fracture toughness of double-aged Al–Zn–Mg–Cu–Ti alloy. It was proposed that fine grain size, dispersion of aging precipitates and smaller width of precipitation free zones (PFZs) may be responsible for higher strength and fracture toughness [23-25].

The grain size was one of the most important parameters for controlling the strength and fracture toughness in recrystallisation microstructures. For 7000 series aluminium alloy, the finer grains will lead to an increase in strength. Moreover, the fracture toughness depends primarily on crack propagation, which has a tendency towards strain localization in grain boundaries. Reduction in grain size was considered to be effective in preventing premature fracture by reducing the dislocation pile-up length in the grain boundaries and exhibited a good performance on fracture toughness [26]. In addition, crystallographic orientation change across a grain boundary could result in crack-plane tilt and twist, and then reduce the effective driving force for crack growth [27]; a smaller grain size introduces more grain boundaries, thus reinforces the role of grain boundary. Fig. 3 presents optical micrograph of the double-aged samples for the fracture toughness tests. Evidently, both alloys exhibit a recrystallized matrix

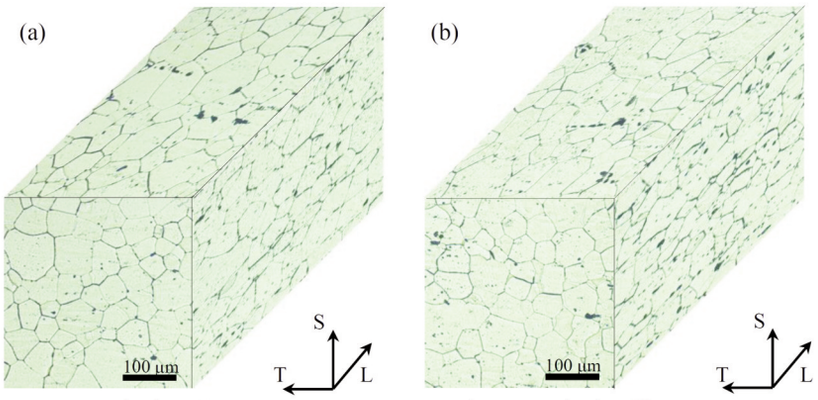

Figure 3. *Optical micrograph of the fracture toughness testing samples (a) Al–Zn–Mg–Cu–Ti alloy; (b) Al–Zn–Mg–Cu–Ti–Sn alloy.*

with feature of nearly equiaxed grains. The average grain size of Sn-containing alloy on T-S plane is 52 μm, measured with the mean linear-intercept method, which is slightly refined and more homogeneous compared with that of the Sn-free alloy (64 μm), indicating that Sn may obstacle growth of recrystallized grains of solution-treated Al–Zn–Mg–Cu–Ti–Sn alloy and result in higher strength and fatigue thoughness.

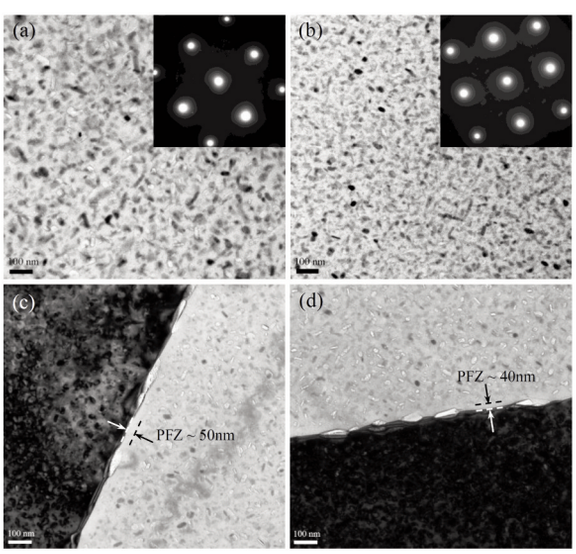

Figure 4. *Images (TEM) and corresponding SAED patterns of double aged Al–Zn–Mg–Cu–Ti(–Sn) alloy in <001>$_{Al}$ (a), (c) grain and grain boundary of Sn free alloy; (b), (d) grain and grain boundary of Sn containing alloy.*

As is known, main precipitates in 7050 aluminium alloy may be G.P zones, η′, and η phases with increasing aging temperature. According to the results in literatures [28-30], the main precipitates inside the grains in peakaged sample are G.P zones and η′, and in the overaged alloy, predominated with η′ and η. Fig. 4 illustrates precipitates and PFZ in the overaged sample, where the fine precipitates are η′ and the rod-like precipitates η. It shows that the Sn-containing alloy has finer and more dispersed η phases. The η particles accounts for a greater proportion within the grain in overaged sample, incoherent with the matrix and are not shearable in nature. The coarser η particles in Sn-free alloy would promote further void formation by means of continued plastic flow around them and these microvoids may contribute to a poor toughness [31].

PFZs beside the grain boundary in overaged alloy also play a significant role on the fracture toughness. The PFZs as soft areas between the matrix and grain boundaries favour concentration of deformation and concomitant microcrack initiation at these regions, moreover, wide PFZs will create additional strain localization, which may encourage grain boundary failure, resulting in facilitating the intergranular fracture [32] and deteriorating the fracture resistance.

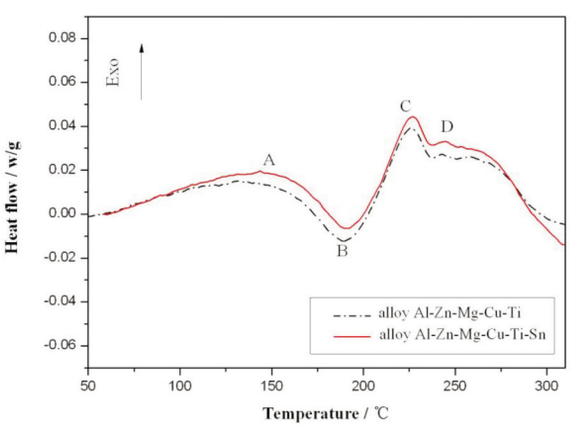

Figure 5. *DSC curves of the experimental alloys after aging at 120°C for 24 h*

As shown in Figs. 4c and 4d, the width of the PFZs in the Sn-containing alloy is narrower than those in the Sn-free alloy. Relatively narrower widths of the PFZs lead to a higher fracture toughness for Sn-containing alloy. In addition, the Sn-containing alloy shows more discontinuous precipitation on grain boundary. This is also believed beneficial to improving grain boundary fracture resistance and fracture toughness of aluminium alloy.

Moreover, Fig. 5 presents the DSC curves of both alloys after solution-treated at 470°C for 1 h then aged at 120°C for 24 h. It is found that both the DSC curves show similar features, suggesting that adding Sn to the Al–Zn–Mg–Cu alloy does not change the type of phase transformation. In light of earlier investigations [2, 33], the first exothermic peak (peak A) can be attributed to formation of η', and the endothermic peak (peak B) corresponds to dissolution of η'. And according to the literature [34], peak C and peak D represent the formation and coarsening of η, respectively. It is seen that, η' in Sn-containing alloy forms and dissolves at a little higher temperature, indicating Sn addition might suppress precipitation and delay dissolution of η'. This explains the delayed appearance and lower peak strength of Sn-containing alloy. Furthermore, peak D shifts to a higher temperature in Sn-containing alloy, providing an evidence for the reduced coarsening of η, which results in the slower over-aged softening and leads to a higher strength of Sn-containing alloy under overaged condition (Fig. 2).

Precipitate coarsening, essentially to say, is related to diffusion of solute atoms. The atomic diffusion in Al–Zn–Mg–Cu alloy is believed to be controlled by vacancy, which is mainly generated during quenching and act as a priority diffusion channel for solute atoms [35]. It has been proposed that the Sn-vacancy binding energy in Al matrix is much higher than that of Mg, Zn and Cu [36]. So the Sn-vacancy pairs reduce the free vacancy concentration in the Al matrix, slowing the diffusion of Mg and Zn atoms, and resulting in finer precipitations in the overaged Sn-containing alloy [37]. Moreover, when bound to Sn atoms, vacancies diffuse difficultly to grain boundaries, contributing to formation of narrow PFZs in the present Sn-containing alloy.

The fracture surfaces of K_{IC} test specimens usually show three basic fracture mechanisms: fracture or decohesion of the coarse constituent particles, intergranular fracture and ductile transgranular fracture, characterized by dimples or large planar areas [38, 39]. Typical fracture surfaces of the failed K_{IC} test specimens under double aging are illustrated in Fig. 6, showing the mixed fracture characteristics of intergranular and transgranular of the Sn-free sample, whereas, the Sn-containing sample is characterized mainly by dimple-type transgranular fracture. The dimples in Sn-containing sample are distributed more randomly throughout the surface and finer and deeper than in Sn-free sample, indicating that the Sn-containing sample obtains a better fracture toughness.

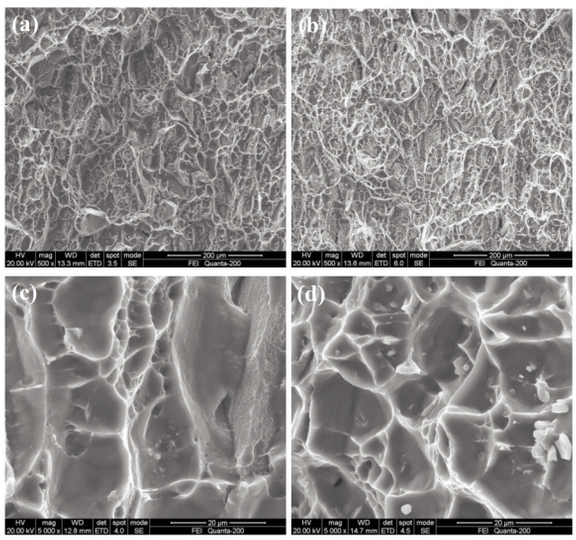

Figure 6. *Fracture surfaces of the failed fracture toughness test specimens under double aging (a), (c) Al–Zn–Mg–Cu–Ti; (b), (d) Al–Zn–Mg–Cu–Ti–Sn.*

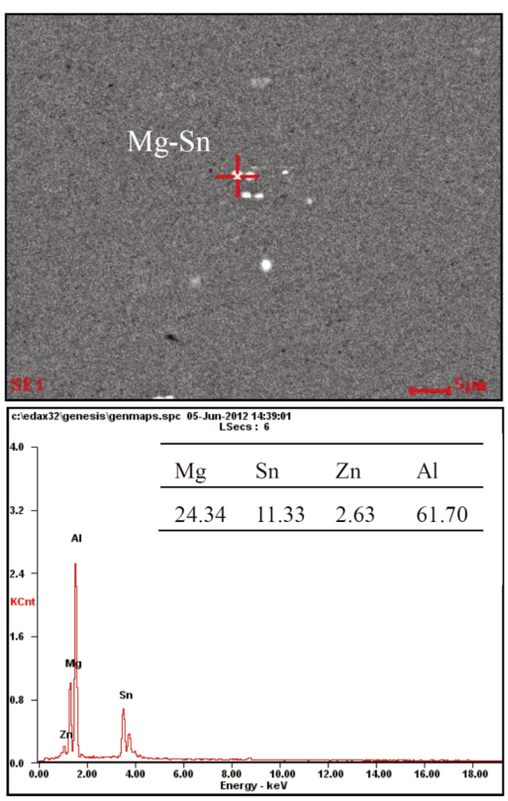

Figure 7. *EDS analysis of Mg-Sn phase in the double aged Sn-containing alloy (at.%)*

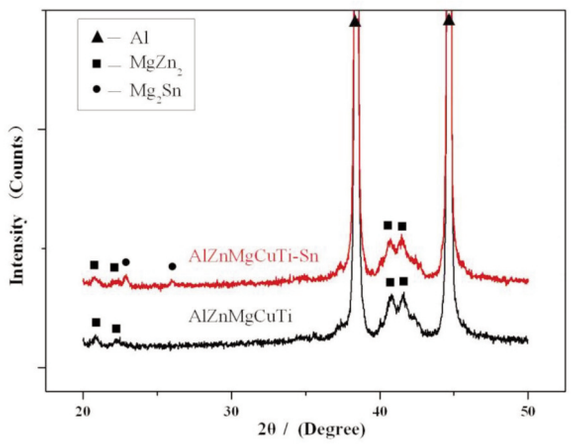

Figure 8. *X-ray diffractometry spectrum of the double aged alloy plate*

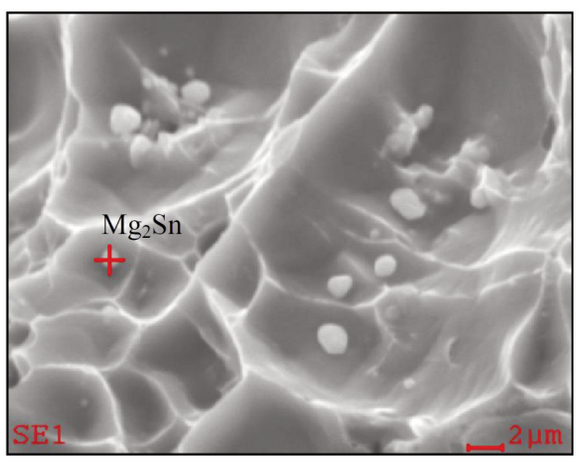

Figure 9. *SEM fractograph showing Mg_2Sn particles associated with dimples*

As shown in Fig. 7, a Mg-Sn phase is presented in the Al–Zn–Mg–Cu–Ti–Sn alloy and the Mg/Sn ratio in this phase is close to 2:1. Fig. 8 shows XRD patterns of the aged alloys, revealing that the Mg-Sn phase should be Mg_2Sn. Mg_2Sn was mainly formed during casting and, if not completely, was not involved in solution-treatment and aging owing to the minimal solubility of Sn in aluminium [40]. Regarding transgranular dimpled rupture, fracture initiation occurred by microvoids nucleation and coalescence. Primary voids are inclined to nucleation on particles interior or particle/matrix interface decohesion. Second phase particles with smaller sizes favors microvoids nucleation [41]. The Mg_2Sn particles can be observed to distribute in the fine dimples (Fig. 9) and was not broken, different from coarse constituent particles which provide a major path for fatigue crack propagation, suggesting that Mg_2Sn may initiate the microvoids and facilitate the dimple formation, thus increase the tendency of dimple-type transgranular fracture and is consistent with toughness improvement.

5. Conclusions

Aging hardening behaviour and fracture toughness of Al–Zn–Mg–Cu–Ti(–Sn) alloys has been studied. Analysis of microstructure reveals that addition of Sn suppresses precipitation, delays dissolution of η' and reduces coarsening of η, leading to the delayed appearance of peak strength and slower over-aged softening of Sn-containing alloy. Moreover, the finer solution-aging grain size and η phase, narrower PFZs and discontinuous distribution of grain boundary precipitates are observed clearly in the double-aged Sn-containing alloy, benefiting to higher strength and fracture toughness. Small size second phase Mg_2Sn shows a useful relationship to the facilitation of dimple-type transgranular fracture and toughness improvement.

Acknowledgement

The authors would like to express their gratitude for the financial support of the Major State Basic Research Development Program of China (grant no. 2010CB731706).

References

[1] T.S. Srivatsan, S. Anand, S. Sriram, V.K. Vasudevan, Mater. Sci. Eng. A, A281 (2000) 292–304.

[2] N. Kamp, I. Sinclair, M.J. Starink, Metall. Mater. Trans. A, 33 (2002) 1125–1136.

[3] C. Mondal, B. Mishra, P.K. Jena, K.S. Kumar, T.B. Bhat, Int. J. Impact. Eng., 38 (2011) 745–754.

[4] I.J. Polmear: Light Alloys: Metallurgy of the Light Metals, 3rd ed., Edward Arnold, London, 1995.

[5] D. Dumont, A. Deschamps, Y. Brechet, Acta Mater., 52 (2004) 2529–2540.

[6] Z. Cvijović, M. Rakin, M. Vratnica, I. Cvijović, Eng. Fract. Mech., 75 (2008) 2115–2129.

[7] O.E. Alarcon, A.M.M. Nazar, W.A. Monteiro, Mater. Sci. Eng. A, 138 (1991) 275–285.

[8] D. Dumont, A. Deschamps, Y. Brechet, Mater. Sci. Eng. A, A356 (2003) 326–336.

[9] V. Singh, K. S. Prasad, A. A. Gokhale, Scripta. Mater., 50 (2004) 903–908.

[10] T. Wirtz, G. Lutjering, A. Gysler, B. Lenczowski, R. Rauh, Mater. Sci. Forum, 331 (2000) 1489–1494.

[11] A.F. Norman, K. Hyde, F. Costello, S. Thompson, Mater. Sci. Eng. A, A354 (2003) 188–198.

[12] F.A. Costello, J.D. Robson, P.B. Prangnell, Mater. Sci. Forum., 396–402 (2002) 757–762.

[13] G.S. Peng, K.H. Chen, H.C. Fang, S.Y. Chen, Mater. Des., 36 (2012) 279–283.

[14] P.C. Bai, T.T. Zhou, P.Y. Liu, Y.G. Zhang, C.Q. Chen, Mater. Lett., 58 (2004) 3084–3087.

[15] Z.W. Huang, M.H. Loretto, J. White, Mater. Sci.

Technol., 9 (1993) 967–980.

[16] S. Tatsuo, H. Shoichi, H. Kiyoshige, Metall. Mater. Trans. A, 34A (2003) 2745–2755.

[17] H.K. Hardy, J. Inst. Met., 80 (1951–1952) 483–492.

[18] S. Banerjee, P.S. Robi, A. Srinivasan, P.K. Lakavatha, Mater. Des., 31 (2010) 4007–4015.

[19] A.M.A. Mohamed, F.H. Samuel, A.M. Samuel, H.W. Doty, S. Valtierra, Metall. Mater. Trans. A, 39A (2008) 490–501.

[20] A. Yan, L. Chen, H.S. Liu, X.Q. Li, Mater. Sci. Technol., 29 (2013) 319-325.

[21] M. Vratnica, G. Pluvinage, P. Jodin, Z. Cvijović, M. Rakin, Z. Burzić, K. Gerić, Mater. Des., 44 (2013) 303–310.

[22] ASTM E399-09. Standard Test Method for Linear-Elastic Plane-Strain Fracture Toughness KIC of Metallic Materials. Philadelphia: American Society for Testing and Materials; 2009.

[23] N.M. Han, X.M. Zhang, S.D. Liu, D.G. He, R. Zhang, J. Alloys Compd., 509 (2011) 4138–4145.

[24] T. Hanlon, Y.N. Kwon, S. Suresh, Scripta Mater., 49 (2003) 675–680.

[25] N. Ryum, Acta Metall., 16 (1968) 327–332.

[26] O.E. Alarcon, A.M.M. Nazar, W.A. Monteiro, Mater. Sci. Eng. A, 138 (1991) 275–285.

[27] S. Suresh, Metall. Trans. A, 14A (1983) 2375–2385.

[28] L.K Berg, J. Gjønnes, V. Hansen, X.Z Li, M. Knutson-Wedel, G. Waterloo, D. Schryvers, L.R Wallenberg, Acta Mater., 49 (2001) 3443–3451.

[29] O.N. Senkov, S.V. Senkova, M.R. Shagiev, Metall. Mater. Trans. A, 39A (2008) 1034–1053.

[30] G. Sha, A. Cerezo, Acta Mater., 52 (2004) 4503–4516.

[31] N.D. Mohammed, R.K. Pandey, A.K. Mukhopadhyay, Mater. Sci. Eng. A, A435–A436 (2006) 318–326.

[32] G.M. Ludtka, D.E. Laughlin, Metall. Trans. A, 13A (1982) 411–425.

[33] J. Buha, R.N. Lumely, A.G. Crosky, Mater. Sci. Eng. A, 492 (2008) 1–10.

[34] J.M. Papazian, Metall. Trans. A, 13A (1982) 761–769.

[35] Y. Mishin, C. Herzig, Acta Mater., 48 (2000) 589–623.

[36] C. Wolverton, Acta Mater., 55 (2007) 5867–5872.

[37] I.A. Figueroa, O. Novelo-Peralta, M.A. Suárez, G.A. Lara-Rodríguez, J. Min. Metall. Sect. B-Metall. 49 (3) B (2013) 293-297.

[38] N.M. Han, X.M. Zhang, S.D. Liu, B. Ke, X. Xin, Mater. Sci. Eng. A, 528 (2011) 3714–3721.

[39] T. Pardoen, D. Dumont, A. Deschamps, Y. Brechet, J. Mech. Phys. Solids, 51 (2003) 637–665.

[40] T.B. Massalski: 'Binary alloy phase diagrams', 2nd edn, Vol. 1, 215; 1990, Materials Park, OH, ASM International.

[41] V.M.J. Sharma, K. Sree Kumar, B. Nageswara Rao, S.D. Pathak, Mater. Sci. Eng. A, 502 (2009) 45–53.